Static and Dynamic Response of Concrete Sleepers

Rikard Gustavson, *Lic.Eng.*
Division of Concrete Structures
Chalmers University of Technology
S-412 96 Göteborg
E-mail: rikard.gustavson@ste.chalmers.se

Kent Gylltoft, Ph.D., Professor
Division of Concrete Structures
Chalmers University of Technology
S-412 96 Göteborg
E-mail: kent.gylltoft@ste.chalmers.se

ABSTRACT

Modern railway traffic may induce highly dynamic loads in railway sleepers. Analytical tools for prestressed concrete sleepers that consider the effects of the dynamic loads are therefore desirable. A finite element model that can be used to conduct both static and dynamic analysis of prestressed concrete sleepers has been developed. Static experiments were conducted and used for a validation model. A track model was used to determine the load that is applied to a sleeper during a train passage. The sleeper response at different train velocities was studied. The accuracy and limitations of static design systems for a concrete sleeper are discussed. The curvature of the sleeper increases in a dynamic load situation, which could lead to increased cracking of the sleeper. A static design system can only be used to design the sleeper for the maximum load level present during a train passage. A dynamic design system is required if a sleeper is to be designed to withstand the load variation during a train passage.

Keywords: Concrete, prestressed sleeper, static and dynamic response, non-linear finite element analysis.

1. INTRODUCTION

In the early stages of railway history, the speeds of trains were quite moderate and the load applied to the track system could be regarded as a static load. However, several research projects have shown that, when the speed and load-carrying capacity of the train become higher, significant dynamic loads are generated due to irregularities of the track and wheels, see e.g. [1,2].

The sleeper has an important role in the track system and it is thereby important that the sleeper is analysed accurately. The traditional philosophy is to use a static design system, where the

static nominal axle load is increased by a dynamic factor. However, several physical phenomena may occur when dynamic loads are applied to concrete sleepers that do not occur under static conditions. For instance, the dynamic loads introduce stress waves in the sleeper, the acceleration of the sleeper introduces inertial forces, and the high strain rate changes the material properties of the concrete. Furthermore, the ballast pressure supporting the sleeper in the track will change with time in a dynamic load situation. The aim of this study was to establish a design system, see Figure 1, where detailed analysis of concrete sleepers can be conducted in both static and dynamic load situations.

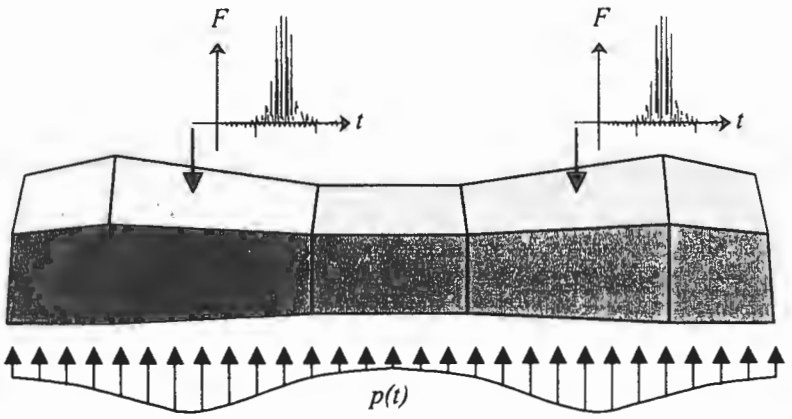

Figure 1 Design system that accounts for the dynamic load situation.

A finite element model of a concrete sleeper was established by use of the non-linear finite element programme Abaqus/Explicit. The finite element model was validated through comparisons with static full-scale test results; thereafter, it was used to investigate the structural behaviour of a sleeper at static load conditions. The finite element model was further extended to involve the sleeper's surroundings and used to determine the effect of dynamic loading on the response of concrete sleepers when placed in a track. The load from a passing train was determined by use of a linear track model based on mode superposition. The extended finite element model was validated through a comparison with results from the track model. The validation is further described in [3]. The possibility and consequences of using a static design system with a dynamic load factor was also studied.

2. EXPERIMENTS

2.1 Test Programme and Arrangements

The aim of the test was to get reliable and practical results to be used as input data and reference data during the establishment and validation of a finite element model, and to examine the failure behaviour of a prestressed concrete sleeper. The results presented in this paper are a selection of the most important results obtained from the tests. A detailed and full presentation of all test results are given in [4].

Six sleepers, manufactured by Abetong Teknik AB, of type A9P, were cut in the middle perpendicular to the line of the sleeper. And each half-sleeper was subjected to a bending moment that produced the same principal deflection shape of the sleeper as if the sleeper were placed in a track system. The test set-up used, see Figure 2, was based on the principles given in [5,6]. The tests were conducted by use of displacement control. The displacement rate used until

the maximum load was reached was 0.05 mm/min. The vertical displacement was measured at the supports and at the loading point, and strain gauges were placed at each side as shown in Figure 2.

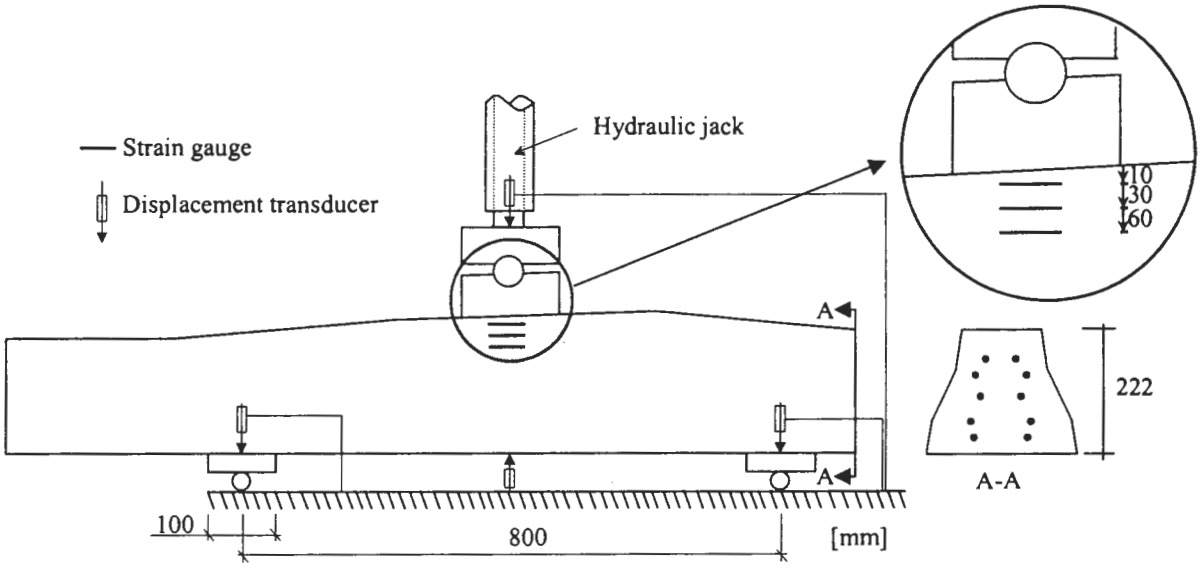

Figure 2 *The test set-up used in the tests.*

Fresh concrete were taken at the sleeper production site in order to cast the tested sleepers and the test specimens (cubes 150x150x150mm, cylinders Φ150x300mm, Rilem beams 100x100x840mm) used to determine the material properties of the hardened concrete. The material properties were determined according to the recommendations of [7,8]. The material properties of the concrete are shown in Table 1. The reinforcement in the concrete sleepers consists of ten steel wires (PC-Strand EU 138/6, 3 x 3.0 mm). The bilinear stress–strain relation of the reinforcement was according to the manufacturer: Young's modulus E_s = 200 GPa, yield strength f_{sy} = 1703 MPa, ultimate strength f_{su} = 1978 MPa, and the strain at maximum stress ϵ_{su} = 6.4 %.

Table 1 *Hardened concrete properties determined from the specimens at the age of 28 days.*

$f_{c,cube}$ (MPa)	$f_{c,cyl}$ (MPa)	E_0 (MPa)	E_c (MPa)	G_F (N/m)
66.0	52.1	31.4	30.2	154

2.2 Test Results

The final failure mode of five of the sleepers was crushing of the concrete combined with failure of the reinforcement; one of the sleepers failed due to anchorage failure. All tested half-sleepers had similar load–vertical displacement relations; see Figure 3. The load–vertical displacement relations were linear until a load of about 135 kN, when cracking was initiated. A non-linear relation was obtained as further cracking occurred. The average maximum load capacity, 263 kN, was reached as crushing and spalling of the concrete in the upper part of the sleeper occurred. A load plateau was reached after the maximum load and was caused by continuous

crushing of the concrete and yielding of the reinforcement, together with small sliding between the reinforcement and the concrete.

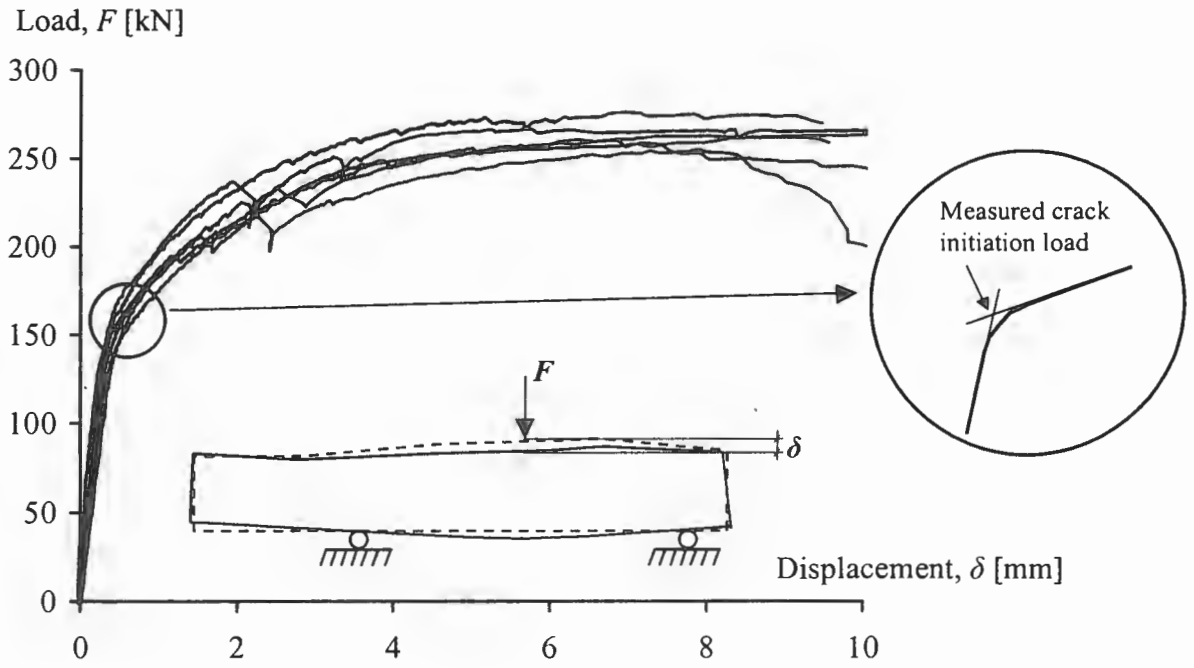

Figure 3 *The load–vertical displacement relation for the six tested half-sleepers and the method for determination of the crack initiation load.*

All sleepers had similar crack propagation during the loading. The first crack was a flexure crack that was initiated at the bottom of the sleeper and appeared parallel to the applied load. As the load was increased, one flexure-shear cracks appeared at each side of the flexure crack at a distance of 160-190 mm. All cracks were initiated at the base of the sleeper and propagated towards the compressive zone beneath the applied load. The bending crack stopped, and the two flexure-shear cracks mended and became almost horizontal as the compressive zone in the top of the sleeper was reached. The characteristic crack pattern obtained in the tests at maximum load is shown in Figure 4.

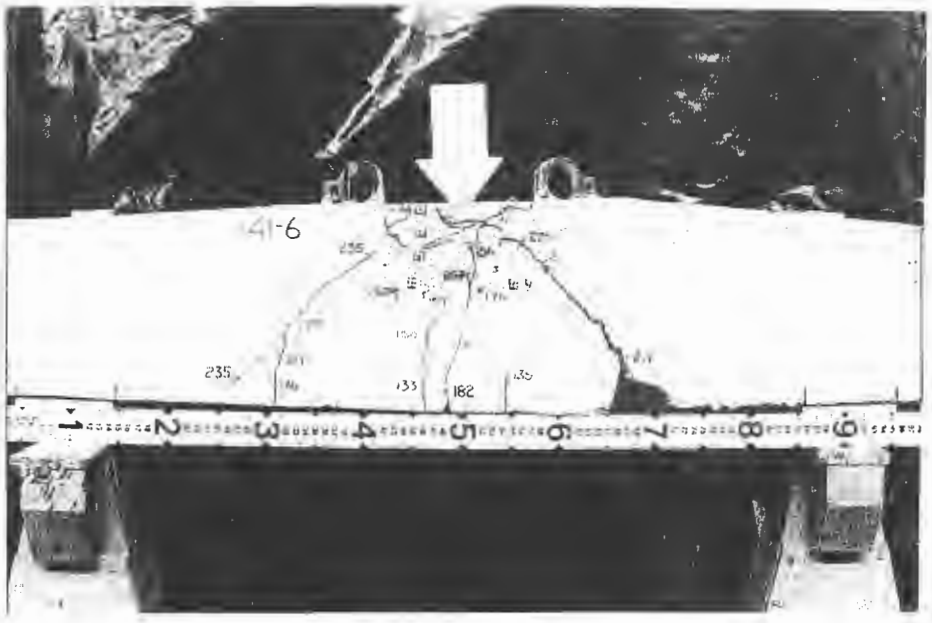

Figure 4 *The characteristic crack pattern obtained in the tests at maximum load.*

The crack initiation load was determined for each half-sleeper from the load–vertical displacement relation. A simplified definition was used in order to obtain a consistent method for the crack initiation load. Crack initiation was defined as the intersection between the load–vertical displacement relations in stages I and II as shown in Figure 3. The method resulted in a slightly higher crack initiation load than if the crack initiation load had been defined as the first deviation from the linear elastic part of the load–vertical displacement relation. The crack initiation load was also detected visually during each test. The average crack initiation loads measured and visually determined were 153 kN and 135 kN respectively.

The height of the compressive zone at failure load was determined from the measurements of the three strain gauges on each side of the half-sleepers. The load–strain relation measured in one of the tests is shown in Figure 5. There it can be seen that the compressive zone at the maximum load ended somewhere between the strain gauges at 30-60 mm. This was similar for all the tested sleepers. The visible signs of crushed concrete at the loading area had a maximum depth of 20 mm from the top surface of the sleeper.

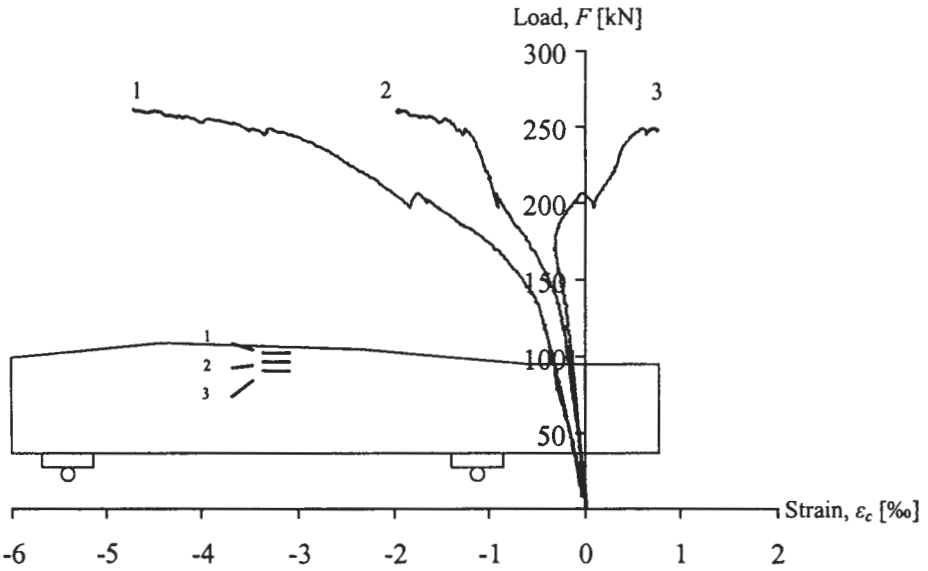

Figure 5 *The positions of the strain gauges at levels 1, 2 and 3 together with the concrete strain at different levels for sleeper 41-1.*

3. NONLINEAR FE-ANALYSES

3.1 The Material Models

The finite element program Abaqus/Explicit version 5.7 used for the analyses in this paper has a concrete material model called *brittle cracking* which is rate-independent and linear elastic in compression, and uses an *elastic-cracking* model to simulate the tensile behaviour; see [9]. The *elastic-cracking* model consists of a crack detection criterion together with an evolution law for the crack. The crack initiation is detected by use of a simple Rankine criterion, which means that a crack is initiated as the maximum principal stress reaches the tensile strength of the concrete. The smeared crack approach was used together with fracture mechanics in order to model the crack evolution. The cracks were smeared out over a characteristic length, determined from the mean crack distance in the tests, of 0.2 m. A bilinear stress–crack opening relation according to

recommendations given in [10] was used to determine the softening of the concrete after crack initiation; see Figure 6.

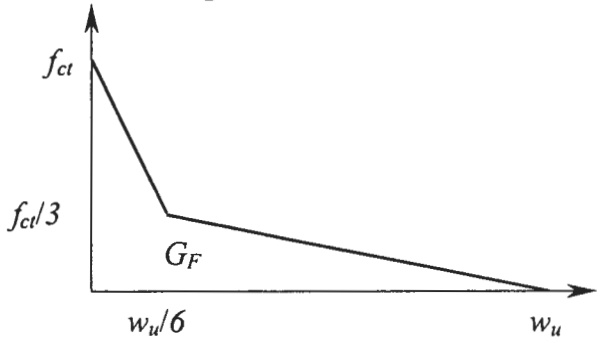

Figure 6 *Bilinear stress–crack opening relation used for simulating the concrete softening. The shape of the relation curve is based on Gylltoft (1983).*

Fixed orthogonal cracks are used in the model. Due to the fixed crack approach, a shear stress relation has to be defined. This is done by a relation between a shear retention factor and the crack opening strain. The shear retention factor is introduced in order to simulate that the crack can still transfer shear stresses until the two crack surfaces are totally separated. A linear relation between the shear retention factor and the crack strain was used in the analyses The shear retention factor was set to 1 when no crack strain was present and 0 at the ultimate crack strain.

Some elements in the numerical model reached stresses high enough to exceed the linear part for compressed concrete, and hence a linear elastic material behaviour is not accurate enough. A rate-independent isotropic *elastoplastic* material model, based on the von Mises yield surface, has been used in order to improve the material modelling of the compressed elements. The uniaxial post-peak stress–strain relation used in the *elastoplastic* model was changed from the uniaxial stress–strain relation obtained in the cylinder tests. The strain values from the tests are determined by consideration of the total length of the test specimen. As localised failure in compression occurs in the elements, a scaling of the strain values is needed in order to simulate the behaviour of the concrete. The ratio between the test specimen length and the element length was used as the scaling parameter according to recommendations given in [11]. The reinforcement is modelled with a plasticity model having a von Mises yield surface.

3.2 The Numerical Model

3.2.1 Modelling of the Concrete and the Reinforcement

Three-dimensional continuum elements were used to model the concrete in the numerical model; see Figure 7. The elements had either eight or six nodes and one integration point as reduced integration was used. In order to model the rather complicated geometry of the half-sleeper and also be able to use a rational reinforcement modelling, a rectangular core with surrounding elements was used. The two different concrete material models above were used in order to capture both crushing and cracking in the sleeper. The dark area at the top of the sleeper shown in Figure 7 was modelled with the *elastoplastic* material model; the rest of the elements were modelled by using *brittle cracking*.

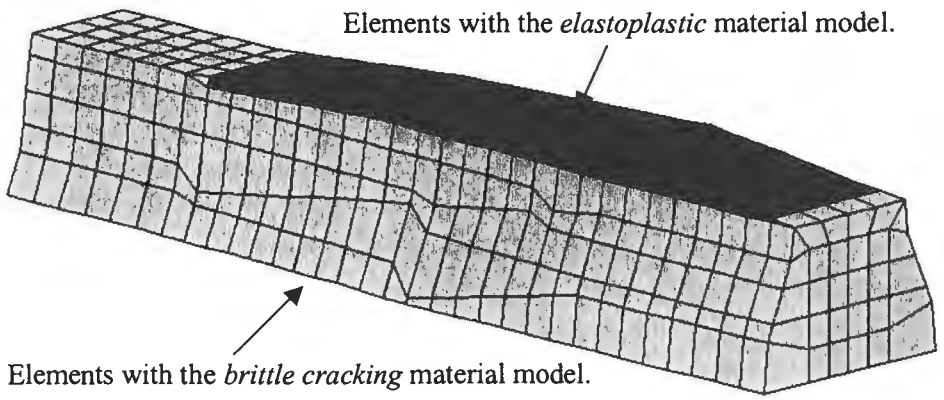

Figure 7 *The two volumes in the sleeper model that are modelled with different concrete material models.*

The reinforcement was included in the concrete structure by an option in Abaqus/Explicit called rebar, which provides an additional stiffness to be added in the direction of the reinforcement bar, and increase the tensile capacity of the element. This modelling assumes that the reinforcement has perfect bonding to the concrete and accordingly the initial variation of the stress in the prestressed reinforcement along the length of the sleeper had to be specified in the model. The transmission length of the reinforcement was estimated according to recommendations given in [12]. The stress in the reinforcement was assumed to increase linearly along the transmission length. The prestress level in the region between the transmission lengths was less than the initial prestress value due to short- and long-term reduction of the prestress in the tendons. The loss of prestress due to shrinkage and creep was estimated according to recommendations given in [13]. A reduction of the initial prestress value by fifteen percent was used as input in the FE-model.

3.2.2 Modelling of the boundary conditions

The load in the tests was applied to the concrete sleeper by the use of a rigid steel plate. The same arrangement was used in the FE-model as the load was applied in the nodes that were placed at the top surface within the area of the rigid steel plate used in the tests. The two steel plates used as supports in the test were included in the model. The interaction between the steel plates and the concrete sleeper was modelled by the use of an interface friction model in the contact zone between the plates and the sleeper. The coefficient of friction at the interface was set to 0.2 according to recommendations given in [14].

3.3 Numerical Results

A validation of the FE-model could be conducted by comparing the structural response in the experimental tests and in the analysis. The finite element programme Abaqus/Explicit, used for all FE-analyses, is mainly used for dynamic analyses. However, the programme has been used for the analyses at static conditions by applying a static load. A detailed study of results from different components and regions of the concrete sleeper shows how well the different types of failure can be captured in the FE-model. In this paper all results from the full-scale tests are shown as a shaded area and the results from the FE-analyses are shown as a solid curve.

The structural response of the concrete sleeper was studied by examining the load–vertical displacement relation. The load–vertical displacement relations from the tests and from the FE-analysis are compared in Figure 8. The non-linear shape of the load–displacement relation from

the tests was due to crack propagation, and crushing of the concrete together with yielding of the reinforcement. This could be simulated with the FE-model, which was able to capture the structural response of the sleeper all the way to the maximum load. The slip between the concrete and the reinforcement, at the load plateau, could not be captured in the FE-model as perfect bonding was assumed between the reinforcement and its surrounding concrete. This, in combination with simultaneous crushing of the concrete and yielding of the reinforcement, caused high accelerations in a few elements in the FE-analysis. Numerical problems occurred in the FE-analysis due to the accelerations and the load plateau could not be captured.

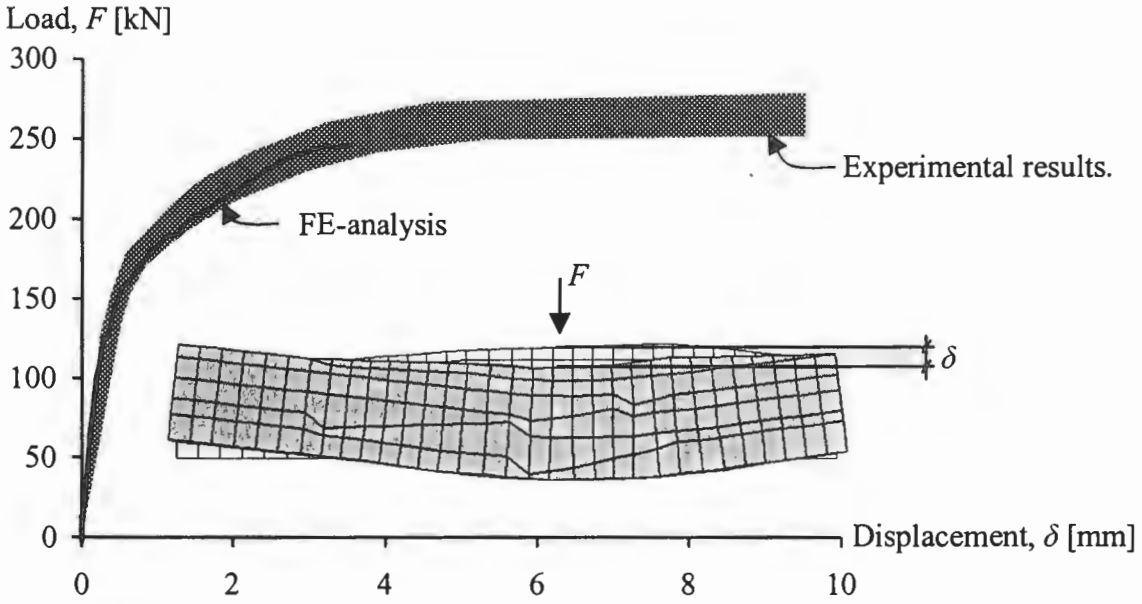

Figure 8 *The load–displacement relation from both the tests and the FE-analysis.*

The height of the compressive zone was examined. Concrete strains from both the tests and the FE-analysis at three different levels according to Figure 9 were used to determine the height of the compressive zone. The load–strain relations from the test and the FE-analysis were not recorded at exactly the same height position, because the integration points of the marked elements in Figure 9 were not at the same vertical positions as the strain gauges in the tests.

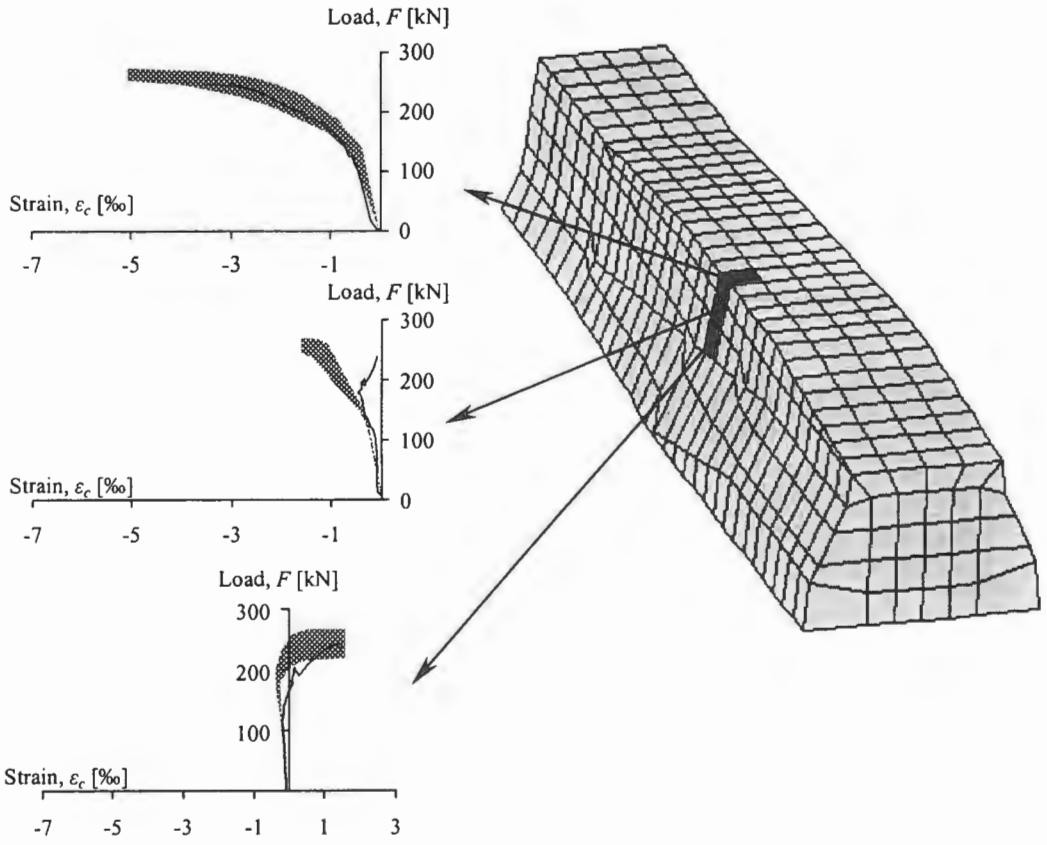

Figure 9 *Concrete strains from the tests and the FE-analysis at three different levels.*

The element mesh could have been established so that the strain-recording levels were matched perfectly. However, this was not considered to be needed as the element mesh used provided enough information concerning the height of the compressive zone. The vertical positions, measured from the top of the sleeper, of the strain gauges in the tests and the integration points in the FE-model are shown in Table 2. The comparison of the concrete strains in Figure 9 shows that there was a fairly good agreement between the test results and the results from the FE-analysis. The height of the compressive zone at failure could be estimated by combining the results from the tests and the FE-analysis. At failure load there was compression at level 2 in the FE-analysis and tension at level 3 in the tests; hence the height of the compressive zone could be estimated to be between 39 and 60 mm. The load–strain relations at level 2 show that there was no need to use a non-linear material model in compression for these elements, as the strain did not exceed the strain value where the concrete response in compression starts to be non-linear. Crushing and spalling of the concrete in the compressive zone were observed in the tests, at the top of the sleeper, to a depth of 20 mm. This zone of the sleeper was modelled with elements that had a height of 24 mm. Results from the FE-analysis at this zone were given by the integration point at level 1. The resulting stress–strain relation in the FE-analysis at level 1 indicated crushing of the concrete as the maximum compressive strength of the concrete was reached; the stress then decreased.

Table 2 *Positions of the three strain-measuring levels.*

Level #	In the FE-analysis [mm]	In the tests [mm]
1	12	10
2	39	30
3	74	60

The propagation of cracks in the sleeper could be studied by examining the evolution of the crack strain magnitude, ϵ^{ck}, which is defined according to equation 1.

$$\varepsilon^{ck} = \sqrt{\left(\varepsilon_{11}^{ck}\right)^2 + \left(\varepsilon_{22}^{ck}\right)^2 + \left(\varepsilon_{33}^{ck}\right)^2} \tag{1}$$

The initiation and propagation of the cracks in the sleeper were similar to the crack history observed in the tests. The first initiation of a crack occurred in the bottom of the sleeper in the line of the applied load. The load at the crack initiation defined as the intersection between stages I and II was 161 kN; the first deviation from the linear elastic part of the load–vertical displacement relation occurred at a load level of 126 kN. Areas with a high crack strain magnitude were developed in line with the vertical and the inclined cracks from the tests throughout the analysis. The contour plot in Figure 10 shows the crack strain magnitude, ϵ^{ck}, at the maximum load reached in the FE-analysis. A bright area indicates a high crack strain magnitude. The extension of the crack pattern from all six tested sleepers is included as encapsulated areas.

Figure 10 *Contour plot of the crack strain magnitude from the FE-analysis at the maximum load together with the crack pattern from the six tests, shown as the encapsulated areas.*

The development of the stresses in the reinforcement was not recorded in the tests but could be studied throughout the FE-analysis. The stress in the reinforcement, in relation to the vertical displacement of the sleeper at a section in the FE-model that was cracked, is shown in Figure 11. The stress level in the reinforcement directly after the stress release was reduced due to longitudinal compression of the sleeper, as part of the stress in the reinforcement was transferred to the concrete. The initial stress value of 1122 MPa in the reinforcement was then reduced to 1076 MPa. The influence of crack initiation on the increase of stress in the reinforcement through the crack can clearly be detected. The stress in the reinforcement increased rapidly when a crack was developed in the sleeper at a vertical displacement around 0.5 mm, and the reinforcement at the bottom of the sleeper was yielding as the ultimate load capacity of the sleeper was approached.

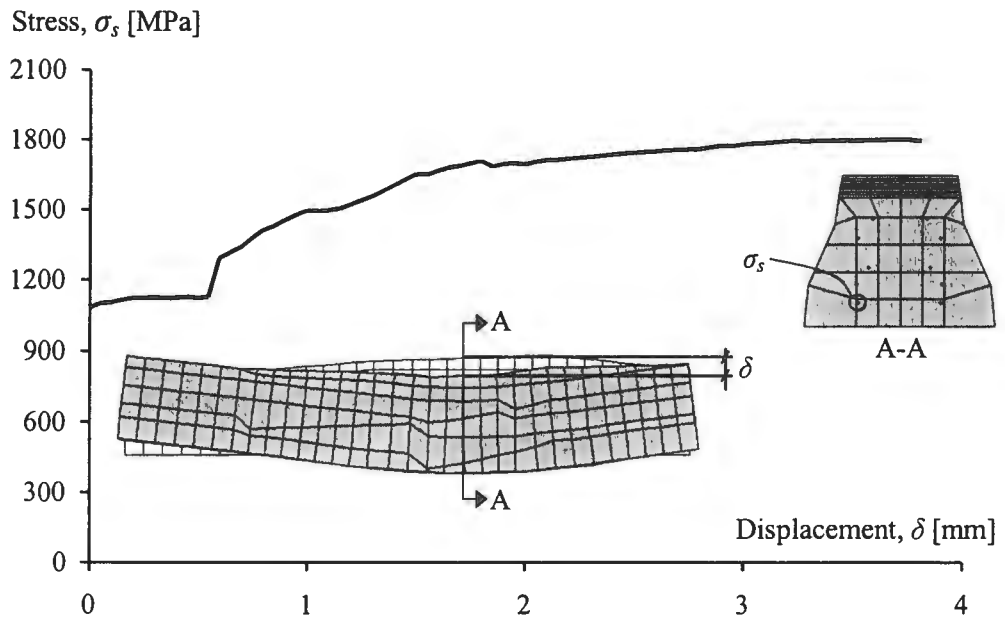

Figure 11 *The stress in the marked reinforcement in relation to the vertical displacement of the sleeper at section A-A.*

3.4 Discussion of Results

The results from the FE-analyses corresponded quite well with the results from the experiments. The stiffness of the structure and the maximum load as well as the crack propagation were similar. The established FE-model was able to capture the structural response of the concrete sleeper involving cracking, crushing and yielding in various zones. The crack propagation could be studied and the stress development in the concrete and the reinforcement steel could be monitored throughout the loading. The main drawback of the FE-model was the lack of bond-slip behaviour between the reinforcement and the surrounding concrete, which caused numerical problems at large deformations. Therefore, the characteristic plateau in the load–vertical displacement relation of a sleeper could not be captured. However, large deformation of the sleeper in the post-elastic range was found not to be present during the train passages studied, which implies that the FE-model could be used to study the non-linear response of a concrete sleeper.

4. SLEEPER STUDIES WITH A DYNAMIC DESIGN SYSTEM

4.1 Prerequisites For the Studies

The FE-model validated for static conditions was established in such a way that it could be used in dynamic analysis where stress waves and time-dependent parameters are present, as a time-dependent solution technique was used. The FE-model of the concrete sleeper was expanded and modified, with use of the knowledge gained in previous studies, to involve the underlying ballast as well; see Figure 12.

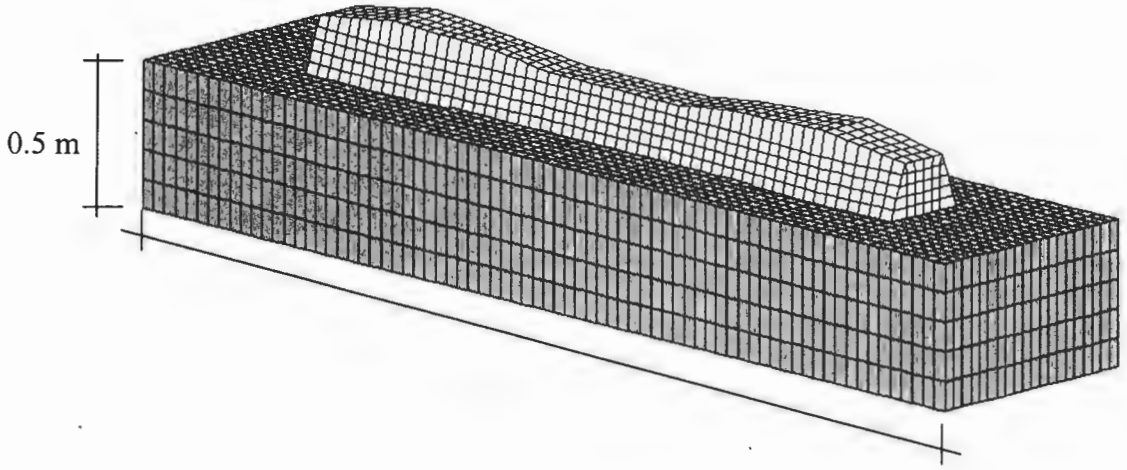

Figure 12 Extended finite element model involving the underlying ballast.

The geometry and material modelling were slightly different from that used in the sleeper model in the previous studies. A small simplification of the sleeper geometry was made in order to get a more evenly distributed element mesh. The material model used for all elements in the sleeper was the *brittle cracking* model in Abaqus/Explicit. This implied that cracking of the concrete could be simulated, but not crushing. However, crushing of the concrete was assumed not to be reached during the train passages studied with this model. The assumption was checked in the analyses and found to be valid. The well-known strain rate effects of concrete and steel, discussed in [3], were not included, as all material models used are strain rate-independent. The reason for this is that the need for strain rate dependence in the material models is limited, since the maximum strain rate, $\dot{\varepsilon}$, obtained in the analysis was approximately 1 s^{-1}. Furthermore, the strain rate has been found to be mesh-dependent, see [11], which leads to approximations concerning the material behaviour that is hard to control.

Contact surfaces were used to simulate the interaction between the sleeper and the underlying ballast. The contact surfaces were defined in such a way that the sleeper was allowed to lift and separate from the ballast volume but not to penetrate into the ballast volume. The contact surfaces implied that, as the sleeper was pressed towards the ballast volume, the contact pressure between the sleeper and the ballast was distributed along the sleeper/ballast interface. The coefficient of friction between the sleeper and the ballast was set to 0.1, which seemed reasonable in order to simulate the existing friction.

The sleeper was studied during train passages at velocities of 130 km/h and 200 km/h, both at quasi-static and dynamic load conditions. In this study a quasi-static load situation was obtained by not introducing any imperfections in the track system, and a dynamic load situation was obtained by introducing a corrugation of the rail surface. The load situation was determined by use of a linear track model called the DIFF-model, where DIFF is an abbreviation of the Swedish "Dynamisk Interaktion Fordon Farbana" (in English, dynamic interaction vehicle track). The railway track in the DIFF-model is modelled as a system of beam members connected with springs and dampers. Different kinds of imperfections on the wheel tread or the railhead can be introduced. The effect of a wheel flat, rail joint, rail corrugation, or rail roughness profile can be studied. Only the vertical train track interaction is considered. A detailed description of the performance and development of the DIFF-model can be found in [15,16].

A track segment with the length of 12 m was modelled in the track model. The chosen length of the track was enough to obtain zero displacement of the sleeper in the midsection of the track segment as the train was positioned at the beginning and at the end of the track. The track length was also enough to minimise the disturbance by the wave reflections at the boundaries of the track model at the position of the studied sleeper. The load from the train was simulated by considering the passage of one wheel. In the simulations at 130 km/h, the train reached the studied sleeper after 0.16 seconds and the duration of the train passage over the track segment was 0.33 seconds. The corresponding values for the simulations at 200 km/h were 0.11 seconds and 0.21 seconds respectively. The depth and the wavelength of the corrugation were chosen in order to induce a dynamic load large enough to cause cracks in the sleepers, 0.7 mm and 0.25 m respectively. Train passage simulations with and without the irregularity as described above were conducted with the track model. The maximum displacement at the train passages with and without rail corrugation at 200 km/h was 0.35 mm and 1.2 mm respectively. The time history of the vertical displacement at the rail seat position of the sleeper, obtained from the track model, was applied to the sleeper in the finite element model. Thereby, detailed non-linear studies of a concrete sleeper placed in a track system and subjected to loads generated by a passing train could be conducted. The principal shape of the vertical displacement–time relation at the rail seat position of the sleeper during a train passage at both quasi-static and dynamic load conditions, at equal velocity of the train, is shown in Figure 13.

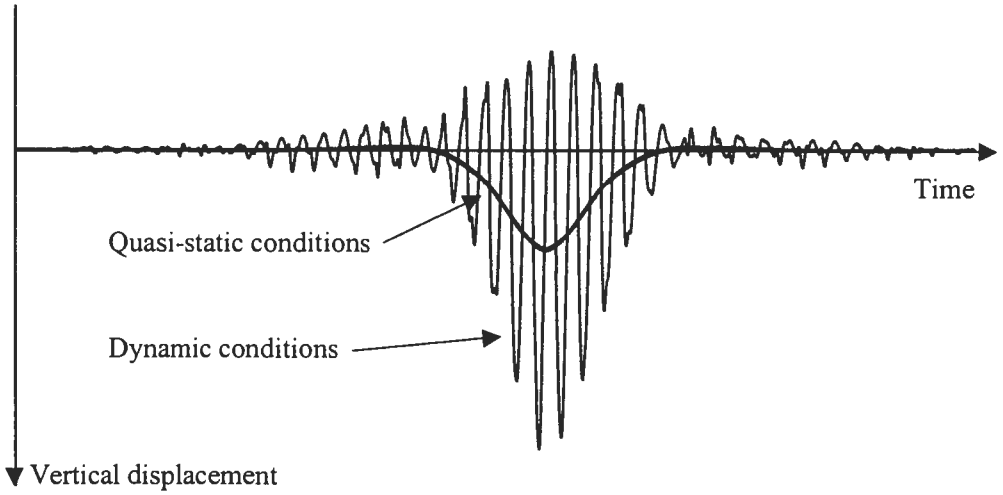

Figure 13 *The principal shape of the vertical displacement–time relation at the rail seat position of the sleeper during a train passage at both quasi-static and dynamic load conditions, at equal velocity of the train.*

4.1 Results from the Studies with the Dynamic Design System

The effect of a dynamic load situation on the response of a concrete sleeper is viewed at a local level in this paper. The effect of cracking in a sleeper on the global response of the entire track structure can be found in [3]. The local response of a sleeper was studied by comparing the response of a sleeper at a 1 mm downward displacement of the rail seat position of the sleeper at different train velocities. This displacement was used for comparison in order to get a clear effect of the displacement rates reached in the simulations at 130 km/h and 200 km/h under both quasi-static and dynamic load conditions. The response of a sleeper at the different displacement rates is shown in Figure 14. At the displacement of 1 mm the reaction force reached was

approximately 200 kN, both in the two quasi-static simulations and in the dynamic simulation at 130 km/h. The reaction force reached in the dynamic simulation at 200 km/h was 230 kN. The increased reaction force was due to the inertial forces that were generated in the sleeper and the underlying ballast. Some inertial forces were also generated in the dynamic simulation at 130 km/h but were found to have a minor effect on the reaction force reached.

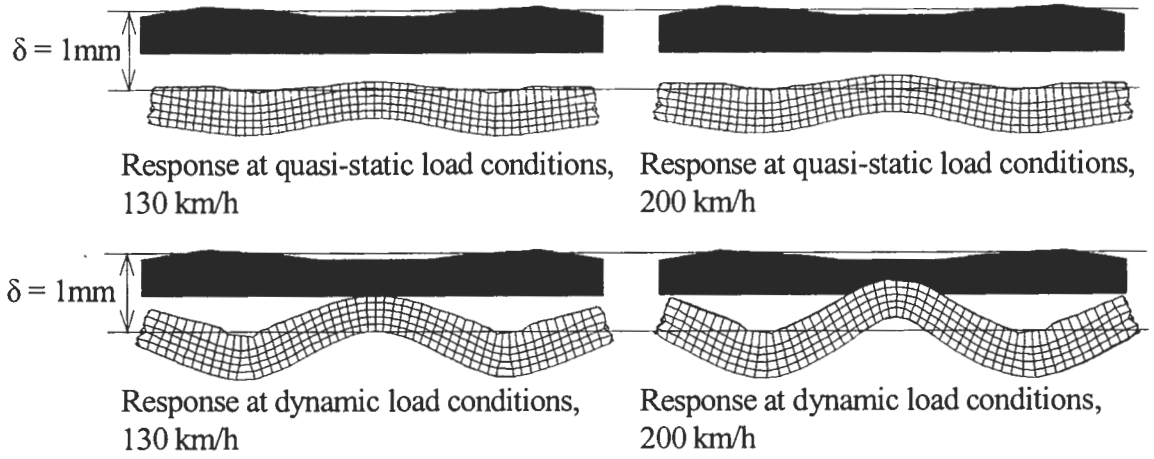

Figure 14 *The response of a sleeper at equal displacement generated in a quasi-static and a dynamic load situation at 130 km/h and 200 km/h (the magnification factor is set to 300).*

The curvature of the sleeper increased as the duration of the load impulse decreased. The explanation of this phenomenon was found as the vertical acceleration within the sleeper was studied. Under quasi-static load conditions, the accelerations were very small and equal along the sleeper. Under dynamic conditions, though, the accelerations were not equally distributed, since large accelerations were generated where the load was applied to the sleeper. The difference in magnitude of the vertical acceleration along the sleeper resulted in an increased curvature, since inertial forces of different magnitude were generated as parts of the sleeper were moved with different velocities. The increase in curvature had large influence on the crack development in the sleeper. The sleepers studied under quasi-static load conditions had no cracks developed at the displacement of 1 mm, but for the sleepers studied under dynamic load conditions the displacement of 1 mm generated cracks in the sleeper. The extent of the cracked areas increased as the velocity of the train was increased. Detailed studies of the initiation, propagation, opening and closing of the cracks in the sleeper were conducted. There were mainly two areas of the sleeper where cracks occurred: at the bottom of the sleeper at the rail seat position, and in the midpoint region at the top of the sleeper. The total crack opening in each cracked area was calculated as the sum of plastic strain times the original length of all the cracked elements. The extension of the existing cracked areas in the sleeper after the train passage is shown in Figure 15, with a contour plot of the crack strain magnitude in the longitudinal direction of the sleeper. The opening and closing of the cracks in the two areas is also shown in Figure 15, by the variation of the total crack opening, w_{tot}, in areas A and B during the train passage.

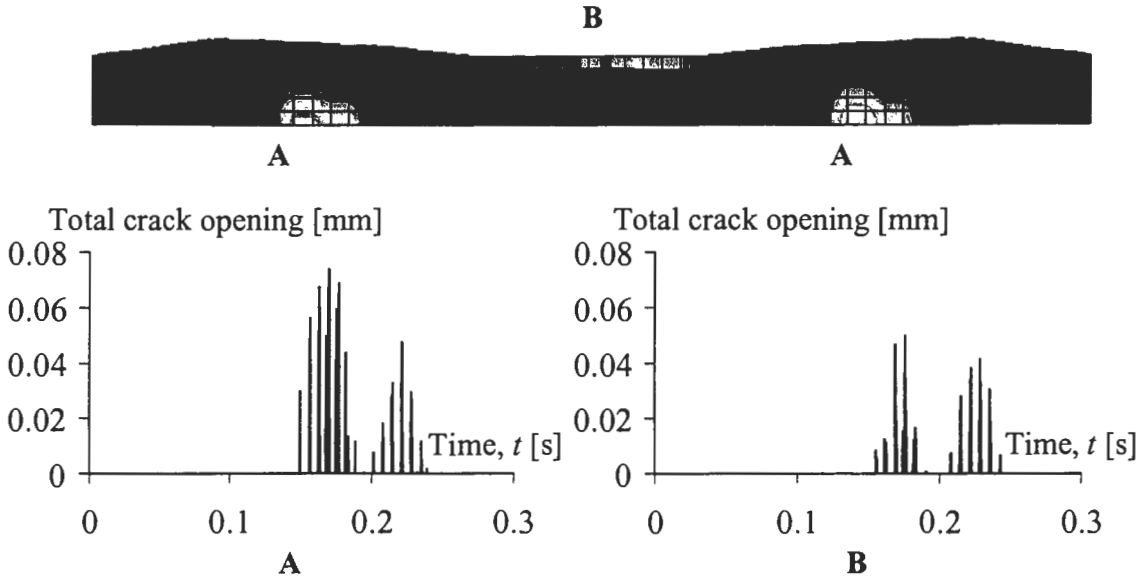

Figure 15 *The existing cracked areas in the sleeper after the train passage, and the opening and closing of the cracks in areas A and B during the passage.*

The study above showed that the duration of each load impulse strongly influenced the local response of the sleeper. However, an increased velocity of the train also had other effects on the local response of the sleeper at dynamic load conditions. The shifts from an upward motion to a downward motion of the sleeper and vice versa were more rapid as the velocity of the train was increased. This had an effect on the distribution and direction of the accelerations in the sleeper. The vertical accelerations in the sleeper during the train passage at 130 km/h were equal in direction, though of varying magnitude, along the sleeper during the train passage. This was mainly the case also during the train passage at 200 km/h, but occasionally the motion of the sleeper shifted very quickly and the direction of the acceleration became different along the sleeper. This led to a curvature of the sleeper that indicated a punching failure of the sleeper at its rail seat positions; see Figure 16. The tendency of concrete structures to shift the failure mechanism from bending to shear or punching failure at impact loading, discussed for instance by [17], could thereby be confirmed in the detailed analyses of the sleeper as vertical accelerations with different directions were present.

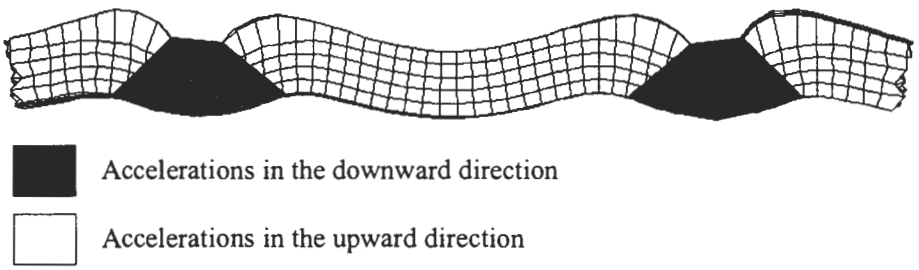

Figure 16 *Indications of a punching failure when accelerations of different directions are present in a sleeper (the vertical displacement magnification factor is set to 300).*

5. THE USE OF A STATIC DESIGN SYSTEM

The studies with the track model showed that if an irregularity is present during a train passage, a highly dynamic load situation might be at hand. The limitations of the static design system, mentioned previously, can thus clearly be seen as this design system only captures the static situation at a load level present during a specific moment. The effects of the variation of the load will thus not be accounted for. The conducted study, where the effect of the velocity of the train is discussed, raises the question of whether the correct curvature of the sleeper is generated in a static design system if a dynamic load factor is used. The curvature of the sleeper in the dynamic analysis depends on the accelerations within the sleeper, and these accelerations will not be present if a static system is used. The simulation with a dynamic load situation where the velocity of the train was set to 200 km/h was used in order to see if the curvature of the sleeper generated in the dynamic analysis could also be obtained in a static analysis. The maximum load, 252 kN, reached in the dynamic analysis with the track model was applied to a sleeper in a static analysis with the sleeper model, and the curvature and the resulting extension of the cracked areas were compared; see Figure 17.

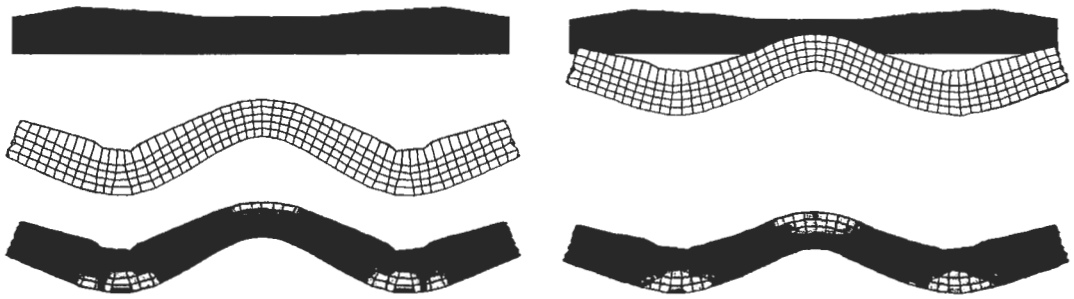

Results from the static analysis Results from the dynamic analysis

Figure 17 *Comparison of results from a static analysis and a dynamic analysis (the magnification factor is set to 200).*

In the static analysis, the applied load resulted in an increased vertical displacement of the entire sleeper. This was due to the absence of inertial forces in the sleeper and the underlying ballast at the static load conditions. Similar curvature and cracking of the sleeper were, however, obtained in the static analysis and the dynamic analysis. This study shows that a dynamic factor can be used in order to design a sleeper only when the sleeper is designed for the maximum reaction force reached during a train passage. However, the effect of the rapid shifts in the motion of the sleeper, discussed previously, is difficult to capture with a static design system.

6. CONCLUSIONS

The structural response of a prestressed concrete sleeper, at both static and dynamic load conditions, was simulated with use of established FE models. Results from static experiments together with the results from FE analyses showed a rather good agreement. The FE model could be used to conduct detailed studies of different areas of the sleeper. As the FE model captured the static response of a concrete sleeper and was based on a time-dependent solution technique, the FE model could be extended to involve the sleeper's surroundings when placed in a track. The sleeper was studied in a dynamic load situation caused by a passing train in the

presence of a rail irregularity. The studies showed that the dynamic load situation is important to consider during the design of a concrete sleeper. The inertial forces induced in the sleeper and the underlying ballast during a train passage result in an increased curvature of the sleeper, which leads to an increased crack propagation. The studies also showed that rapid shifts from an upward motion to a downward motion of the sleeper and vice versa could lead to a punching failure of the a sleeper. The study with the dynamic design system shows that a static design system can only be used to ensure that a sleeper withstands a specific load level at static conditions. The effects from fast reversible loads, such as the load from a passing train, can be considered only if a dynamic design system is used.

7. REFERENCES

1. Buekett J., Firth D., Surtees J. R. (1987): *Concrete ties in modern track.* Railway Track and Structures (RT&S), Vol. 83, No. 8, August 1987, pp. 32, 34-35, 37.

2. Wakui H., Okuda H. (1991): *Effects of wheel-flats on concrete sleepers.* International Symposium on precast concrete railway sleepers, Madrid, 1991, pp. 287-299.

3. Gustavson, R. (2000): *Static and dynamic finite element analysis of concrete sleepers*, Publication 00:3, Chalmers University of Technology, Division of Concrete Structures, Göteborg, March 2000, 76 pp. (No. 41), Licentiate Thesis.

4. Gustavson R. (1999): *Concrete sleeper subjected to static loading: An experimental study*, Division of Concrete Structures, Chalmers University of Technology, Göteborg, Sweden, Report 99:4, 32 pp.

5. Gylltoft K. (1979): *Utmattningsprovningar av betongsliprar.* Division of Structural Engineering, Luleå University of Technology, Sweden, Report R103:1978, 91 pp.

6. Sjödahl O. (1995): *Sliprar av betong.* Tekniska bestämmelser. Föreskrift rörande Banverkets sliprar. Banverket. HK. TMS. BVF 522.32, 6 pp.

7. BST Byggstandardiseringen (1991*): Betongprovning med Svensk Standard, BST handbok 12, utgåva 6* (Swedish Standards for Concrete Testing, BST handbook 12, sixth edition. In Swedish). SIS – Standardiseringskommissionen i Sverige och Svensk Byggtjänst, Stockholm, Sweden, 286 pp.

8. RILEM 50-FMC Committee (1985): *Determination of the fracture energy of mortar and concrete by means of three-point bend test on notched beams*, Materials and Structures, Vol. 18, pp. 285-290.

9. HKS (1998): *ABAQUS/Explicit Version 5.7.* Hibbit, Karlsson and Sorensen Inc. Pawtucket, RI.

10. Gylltoft K. (1983): *Fracture mechanics models for fatigue in concrete structures*, Division of Structural Engineering, Luleå University of Technology, Doctoral thesis 1983:25 D, Luleå, 210 pp.

11. Johansson M. (2000): *Non-linear finite-element analyses of concrete frame corners*, Journal of Structural Engineering, Vol. 126, No. 2, February 2000, pp. 190-199.

12. Design Handbook (1998): *High Performance Concrete Structures. Design Handbook* (edited by L. Apleberger, K. Cederwall, M. Grauers and K. Nylander), Division of Structural Engineering, Luleå University of Technology, Luleå, 1998, 110 pp.

13. Engström B. (1996): *Beräkning av förspända betongkonstruktioner*, Division of Concrete Structures, Chalmers University of Technology, Göteborg, Sweden, January 1992, Kompendium 96:1, 186 pp.

14. Boverket (1994): *Boverkets handbok för betongkonstruktioner BBK 94, Band 1, Konstruktion* (Boverkets Handbook for Concrete Structures, BBK 94, Vol. 1, Design. In Swedish). Boverket, Byggavdelningen, Karlskrona, Sweden, 185 pp.

15. Nielsen J. C. O. (1993): *Train/Track Interaction, Coupling of moving and stationary dynamic systems – Theoretical and experimental analysis of railway structures considering wheel and track imperfections*. Division of Solid Mechanics, Chalmers University of Technology, Göteborg, Sweden, November 1993, 97 pp.

16. Oscarsson J. (1999): *Dynamic train/track/ballast interaction, Linear and state-dependent track models*. Department of Solid Mechanics, Chalmers University of Technology, Göteborg, Sweden, February 1999, 62 pp.

17. Wang N. (1996): *Resistance of concrete railroad ties to impact loading*. Department of Civil Engineering, University of British Columbia, Vancouver, Canada, May 1996, 248 pp.